This is a repository copy of *An analytical approach to modelling shear panels in steel beams at elevated temperatures*.

White Rose Research Online URL for this paper:
http://eprints.whiterose.ac.uk/84156/

Version: Accepted Version

Article:
Quan, G., Huang, S. and Burgess, I. (2015) An analytical approach to modelling shear panels in steel beams at elevated temperatures. Engineering Structures, 85. 73 - 82. ISSN 0141-0296

https://doi.org/10.1016/j.engstruct.2014.12.016

Reuse
Unless indicated otherwise, fulltext items are protected by copyright with all rights reserved. The copyright exception in section 29 of the Copyright, Designs and Patents Act 1988 allows the making of a single copy solely for the purpose of non-commercial research or private study within the limits of fair dealing. The publisher or other rights-holder may allow further reproduction and re-use of this version - refer to the White Rose Research Online record for this item. Where records identify the publisher as the copyright holder, users can verify any specific terms of use on the publisher's website.

Takedown
If you consider content in White Rose Research Online to be in breach of UK law, please notify us by emailing eprints@whiterose.ac.uk including the URL of the record and the reason for the withdrawal request.

eprints@whiterose.ac.uk
https://eprints.whiterose.ac.uk/

Graphical Abstract (for review)

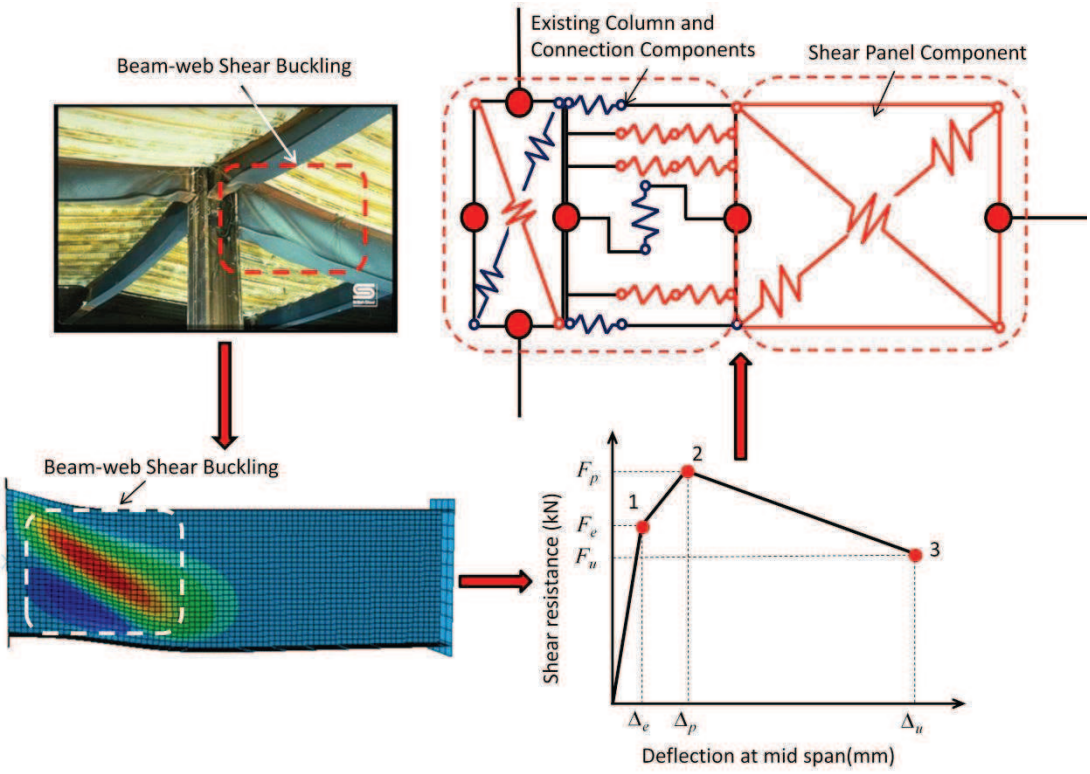

***Highlights (for review)**

Click here to download Highlights (for review): Highlights.docx

- Theoretical model to investigate shear buckling of Class 1 beams in fire.
- Shear buckling occurs mainly in short beams.
- For long beams, bottom flange buckling happens instead.
- Shear resistance reaches its peak when plastic buckling starts.
- In post-buckling shear resistance of the panel decreases.

*Abstract
Click here to download Abstract: Abstract.docx

Abstract

Shear buckling of beam webs in the vicinity of beam-to-column connections has been observed in many full-scale fire tests. This phenomenon can lead to force redistribution within the adjacent connections, and even influence the performance-based analysis of full-scale structures in fire. However, beam-web shear buckling for Class 1 beams at either ambient or elevated temperatures has not been well studied previously. In this work an analytical model has been created to predict the shear buckling behaviour of Class 1 beams in the vicinity of beam-to-column connections at ambient and elevated temperatures. The model considers the reduction of resistance of the beam after web shear buckling has occurred. It is capable of predicting the shear resistance and transverse drift of the shear panel from its initial loading to final failure. Several 3D finite element models have been created using the ABAQUS software, in order to validate the analytical model over a range of geometries. Comparisons between the theoretical and FE models have shown that the proposed method provides sufficient accuracy to be implemented and used in performance-based global modelling.

*Manuscript
Click here to download Manuscript: Revised Manuscript.docx Click here to view linked References

Title: An Analytical Approach to Modelling Shear Panels in Steel Beams at Elevated Temperatures

Authors: Guan Quan, Shan-Shan Huang, Ian Burgess

Address: Department of Civil and Structural Engineering, Sir Frederick Mappin Building, Mappin Street, Sheffield, S1 3JD

Email: g.quan@sheffield.ac.uk

Tel: 01142225726

Fax: 01142225700

Keywords: Shear buckling; Connections; Component-based model; Fire.

An Analytical Approach to Modelling Shear Panels at Elevated Temperatures

Guan Quan, Shan-Shan Huang, Ian Burgess
University of Sheffield, Department of Civil and Structural Engineering, UK

Abstract

Shear buckling of beam webs in the vicinity of beam-to-column connections has been observed in many full-scale fire tests. This phenomenon can lead to force redistribution within the adjacent connections, and even influence the performance-based analysis of full-scale structures in fire. However, beam-web shear buckling for Class 1 beams at either ambient or elevated temperatures has not been well studied previously. In this work an analytical model has been created to predict the shear buckling behaviour of Class 1 beams in the vicinity of beam-to-column connections at ambient and elevated temperatures. The model considers the reduction of resistance of the beam after web shear buckling has occurred. It is capable of predicting the shear resistance and transverse drift of the shear panel from its initial loading to final failure. Several 3D finite element models have been created using the ABAQUS software, in order to validate the analytical model over a range of geometries. Comparisons between the theoretical and FE models have shown that the proposed method provides sufficient accuracy to be implemented and used in performance-based global modelling.

Keywords: Shear buckling; Connections; analytical model; Fire.

Notation:

b_f	Flange width
c	Distance between plastic hinges along the bottom flange
d	Height of a beam web
e	Length of an arbitrary tensile strip
E	Young's modulus at ambient temperature
G	Shear modulus at ambient temperature
f	Width of one strut in compression zone
$f_{p,\theta}$	Stress at the proportional limit
$f_{y,\theta}$	Yield strength of steel at elevated temperatures
F_e	Shear resistance of the beam at the end of elasticity
F_p	Shear resistance of the beam at the initiation of plastic shear buckling
F_u	Ultimate shear resistance of the beam
h_c	Height of the area resisting axial force in a strut
I	Second moment of area of a cross-section
$k_{E,\theta}$	Reduction factor for Young's modulus
l	Half length of the beam
L	Full length of a beam
m	Distance between the beam-end plastic hinge and an arbitrary tensile strip
M_0	Plastic bending moment capacity of one flange
M_1	Reduced plastic bending moment capacity of one flange
M_p	Bending moment resistance of one strut
M_r	Bending moment at the end of the beam
n	The distance between two end points of a tensile strip in Region B along the deformed flange
P_c	Axial force resistance of one strut
q	Uniformly distributed load on the top flange of the beam
t	Thickness of the beam web
t_f	Thickness of the flange
W_{At}	The internal work of tensile strips in Region A
W_{Bt}	The internal work of tensile strips in Region B
W_C	The internal work of the beam web caused by compression
W_e	The external work of the beam
W_f	The internal work of the plastic hinges on the beam flanges
W_T	The internal work of the beam web caused by tension
W_W	The internal work of the beam web
α	The angle between tensile strips and the deformed upper flange
γ	The angle between diagonal of the shear panel and deformed upper flange
δ_e	Elongation of an arbitrary tensile strip
δ_{tA}	Elongation of the tensile strip in Region A
δ_{tB}	Elongation of the tensile strip in Region B
Δ	Out-of-plane deflection of one strut
Δ_e	Mid-span deflection at the end of elasticity
Δ_p	Mid-span deflection at the initiation of plastic shear buckling
Δ_{rB}	The resultant movement of the right point of the representative strip in Region B
Δ_{rs}	The resultant movement of the right edge of the shear panel
Δ_u	Ultimate mid-span deflection
Δ_{vb}	Mid-span deflection caused by bending moment

Δ_{vB}	The vertical movement of the right point of the representative strip in Region B
Δ_{vm}	The vertical movement of the mid span caused by shear force
Δ_{vs}	The vertical movement of the right edge of the shear panel
$\varepsilon_{l,\theta}$	Limiting strain for yield strength
$\varepsilon_{p,\theta}$	Strain at the proportional limit
ε_t	Tensile strain of a tensile strip
$\varepsilon_{u,\theta}$	Ultimate strain of steel
$\varepsilon_{y,\theta}$	Yield strain of steel
θ	The angle between deformed upper flange and horizontal line
σ_c	Compressive stress in the compressive strips
σ_t	Tensile stress in the tensile strips
τ	Average shear stress along the cross section

1. Introduction

The official investigation [1] of the collapse of the '7 World Trade' building in New York City has indicated that the collapse of the building was triggered by the failure of beam-to-column joints after prolonged exposure to fires. Joint failure may initiate fire spread within a building, or even progressive collapse of the whole building. Hence, the joints are among the most critical structural elements of a steel or composite framed building in fire conditions. A considerable body of research related to the modelling of joints in fire has been carried out during the last three decades [2-4]. The Cardington Fire Tests [5] indicated that the shear buckling of beams in the vicinity of beam-to-column joints, is very prevalent under fire conditions, as shown in Fig. 1, which shows shear buckling from the well-known Cardington full-scale tests. For a column-face joint, the effect of shear buckling of the beam web, which increases the transverse drift of the beam, can change the force distribution in the joint components themselves. Conversely, beam-web shear buckling, which leads to an increase of beam deflection, can be advantageous, as it may reduce the net tying force in the joint. Considering the same vertical force component, a lower local resultant shear force exists along the beam when it is acting essentially as a catenary cable. However, nearly all the existing research on joints has neglected the contribution of the shear buckling behaviour in the vicinity of beam-ends. Therefore, it is useful to be able to predict beam-web shear buckling behaviour in fire, and to include this effect in full-structure design modelling, which can be used with a view to preventing progressive collapse.

In this paper, the shear buckling behaviour of the beam web has been studied. An analytical model has been developed to predict the behaviour of shear panels for Class 1 beams, at

both ambient temperature and elevated temperatures; in developments of the work this can be used to generate a component-based shear-panel element. The analytical model can initially evaluate the distance between plastic hinges on the flanges, and then reasonably predict shear capacity and vertical deflection of the shear panel. A range of 3-dimensional finite element models has been created using ABAQUS. These models can be used to produce force-transverse deflection relationships which are necessary to validate the analytical model over a range of geometries. The results from the analytical model will be seen to agree well with the ABAQUS results. As the shear stiffness of the shear panel changes significantly due to beam-web shear buckling, a new component-based shear panel element, which considers the shear panel as a separate component, will be created based on the analytical model, as shown in Fig. 2.

Since no practical research has been done on the post-local-buckling behaviour of Class 1 beams at either ambient or elevated temperatures so far, the analytical model is based on the classic "tension field theory" of plate girders. This has been adapted to the structural response of Class 1 beams, which can form a plastic hinge with the rotation capacity required by plastic analysis, without reduction of its resistance according to Eurocode 3 Part 1-1 [6]. A brief review of the development of tension field theory is presented in the next section.

2. Brief review on the tension field theory of shear web panels

As early as 1886, the possibility of utilizing the post-buckling strength of plate in bridges was considered by Wilson [7]. Later Wagner [8] presented a diagonal tension theory concerning buckling and post-buckling behaviour for aircraft structures in 1931. However, the post-buckling behaviour of beam web panels was not considered as a design concept until the

1960s; until this time the elastic buckling load was used as the only design limit criterion. In the 1960s, Basler *et al.* [9-11] presented a method of calculating the post-buckling capacity of the webs of plate girders subject to shear; this work was later used as the basis of a design method [12] introduced by the American Institute of Steel Construction (AISC). However, in this theory, the flanges of plate girders were assumed to be too flexible to carry significant bending moments, which led to conservative results. Subsequently, Fujii [13] presented a modification of Basler's theory, considering the contribution of flanges to the total post-buckling load capacity. In the 1970s, Rockey *et al.* [14-17] presented a systematic study of, and a design method for, plate girders subject both to pure shear and to combined shear and bending. Their theory further improved Basler's theory by considering the strength of flanges. The theories above are all classified as 'tension field theory' or its derivatives, because the fundamental assumption is that, after elastic buckling, any additional load is carried by a tensile membrane field. Tension field theory only deals with web panels with aspect ratios less than 3 [18]. Hereafter, the term 'aspect ratio' refers to the ratio of the distance between adjacent transverse stiffeners to the depth of the web panel. The theory was later shown, by Lee and Yoo [19], to be able to predict well the post-buckling strength under pure shear of panels of aspect ratios smaller than 1.5, but to lose accuracy for higher aspect ratios. This indicates that tension field theory should only be used to represent plate girders with transverse stiffeners. Lee and Yoo [19-21] carried out a series of finite element studies to investigate the post-buckling behaviour. They modified the existing formulations to decrease the discrepancy between tension field theory and their finite element modelling. They also proposed empirical amendments to classical tension field theory for web panels with aspect ratios higher than 3. Vimonsatit *et al.* [22, 23] extended the classical ambient-temperature tension field model for plate girders, to

account for elevated-temperature behaviour, by changing material properties and incorporating the effect of compressive forces due to axial restraint.

3. Development of the analytical model

Classical tension field theory can represent the post-buckling behaviour of plate girders very well [9-11, 14-17]. In these models, shear resistance involves three stages: pre-buckling, post-buckling and collapse. In the pre-buckling stage, no buckling appears in the panel, and the principal tensile and compressive stresses are identical until elastic buckling happens. The elastic buckling strengths of plates under various conditions are given by Timoshenko [24]. In the post-buckling stage, stress redistribution occurs, with increase occurring especially in the directions of the tensile principal stresses. Any additional compressive stress after web shear buckling can effectively be neglected. In the collapse stage, four plastic hinges appear on the flanges, and finally the plate girder fails in a "sway" mechanism. In the proposed analytical model, for Class 1 beams, the shear response once again consists of three stages, which differ from those of tension field theory. These are the elastic, plastic and plastic post-buckling stages. The behaviour of the web panel of a Class 1 beam subject to shear and bending moment is compared with that of a plate girder in Fig. 3.

The aim of the proposed model is to produce a tri-linear force-displacement relationship for any shear panel, from initial loading to failure. An example characteristic is shown schematically in Fig. 4.

In this figure, Point 1 illustrates the end of the pre-buckling elastic stage. In the elastic stage, it is assumed that no buckling appears in the panel, and the principal tensile and compressive stresses are identical. The beam-end reaction force is calculated on the basis of the design elastic shear resistance according to Eurocode 3 Part 1-1 [6]. Up to Point 1, the

mid-span vertical deflection of a beam is assumed to be induced by both bending and shear. Therefore, Eurocode 3 can be used to calculate the shear resistance and deflection at this point. Point 2 refers to the initiation of buckling, and Point 3 represents failure. The failure here is only a defined point to put an end to the force-deflection curve of the analytical model with a strain too large to be reached by beams in a real fire scenario; it does not necessarily represent a real failure. In the analytical model, the strain 0.15, which is the end of plateau in the material stress-strain characteristic according to Eurocode 3 [25], has been used in the calculation of Point 3. As the object of the study is beam-web shear buckling, for all the beams analysed, resistance to shear is more critical than to bending moment. Therefore, the resistances below all refer to shear resistance. Bending moment is assumed to be solely resisted by the top and bottom flanges. The shear resistance and the mid-span vertical deflections at Points 2 and 3 are to be evaluated by the proposed analytical model.

In the calculation procedure, several assumptions have been made for the post-buckling phase.

(1) The four edges of the shear panel are assumed to be rigid.

(2) The panel is composed of tensile strips aligned at 45^{o} to the horizontal and compressive strips perpendicular to these tensile strips (see Fig. 3(f)). The stresses within all the tensile strips are identical, as are the stresses within all the compressive strips.

(3) The stress-strain relationship for structural steel at high temperatures is based on Eurocode 3 Part 1-2 [25], for which the model is shown in Fig. 5(b); however the curvilinear inelastic development phase of the Eurocode curve is replaced by a sharp transition from elasticity to plasticity, as only the two end points of the sharp transition (corresponding to proportional limit state and the initiation of yield state)

have been used in the analytical model; the path in between these two points does not affect the result of the key points in the analytical model. The reduction factors for yield strength and Young's modulus at high temperatures from this code have been used in the analytical model. At ambient temperature, the stress-strain relationship is based on the same general constitutive model. To be consistent with the stress-strain relationships at high temperatures, the same limiting strain at yield $\varepsilon_{l,\theta}$ and the same ultimate strain $\varepsilon_{u,\theta}$ are applied to the stress-strain curve at ambient temperature. The stress-strain relationship for structural steel at ambient temperature is shown in Fig. 5(a).

3.1 The deflection at mid-span

It has been mentioned above that, at Point 1, the mid-span vertical deflection of a beam is assumed to be induced elastically by bending and shear. The mid-span deflections at Points 2 and 3 both consist of a summation of the transverse drift of the shear panel due to shear force and the deflection caused by curvatures due to bending moment.

The analytical model assumes that the mid-span deflection cause by bending moment from Point 1 to Point 3 can be calculated as Eq. (1).

$$\Delta_{vb} = \frac{qL^4}{384 k_{E,\theta} EI} \tag{1}$$

While the deflection caused by shear force can be derived as Eq. (2)

$$\Delta_{vm} = \frac{\tau}{k_{E,\theta} G} \times l \tag{2}$$

For the transverse drift caused by shear buckling, it is assumed that the tensile strains of the tensile strips within the whole panel are identical. Thus, only the tensile strain of one representative tensile strip AB is calculated, as shown in Fig. 6.

For tensile strips,

$$\varepsilon_t = \frac{\delta_e}{e} \tag{3}$$

$$e = \frac{\sqrt{c^2 - \Delta_{vs}^2}}{\cos(\alpha + \theta)}, \quad \delta_e = \Delta_{vs} \frac{\sin\alpha}{\cos\theta} \tag{4}$$

Substituting Eq. (4) into Eq. (3) gives

$$\varepsilon_t = \Delta_{vs} \frac{\sin\alpha \cos(\alpha + \theta)}{\sqrt{c^2 - \Delta_{vs}^2}\cos\theta} \tag{5}$$

For Point 2, it is assumed that the principal tensile strain at an arbitrary point within the shear panel is 0.02, which is the yield strain in the material stress-strain relationship according to Eurocode 3 [25]. For Point 3, the strain at the arbitrary point is 0.15. Therefore, for any given distance c between plastic hinges on the flanges, the mid-span vertical deflection for Points 2 and 3 can be calculated. The key is to evaluate c.

3.2 Shear resistance of the beam

The calculation principle below is based on the equality of the internal plastic work and the external loss of potential energy of the load. Following this calculation, the distance between the plastic hinges can be calculated in order to fulfil the work equilibrium and to correspond to the smallest uniformly distributed load q. The method of calculating the internal work of the beam and the external loss of potential of the applied force is shown below.

3.2.1 Internal work of the beam web

It is assumed that the shear panel is composed of tensile and compressive strips, as shown in Fig. 3. Although the directions of both the tensile and compressive strips are initially defined in the second assumption above, the locations of the plastic hinges on the flanges

are unknown. There are three possible cases, as shown in Fig. 7, which may affect the internal work done by the tensile and compressive strips.

3.2.1.1 Case 1

In Case 1, as shown in Fig. 8(a), the angle α is smaller than diagonal angle γ.

In Region B, for an arbitrary strip EF, the relationship between the elongation δ_{tB} of the strip and the resultant movement Δ_{rB} of Point F (as shown in Fig. 8(b)), is

$$\delta_{tB} = \Delta_{rB} \sin\alpha \tag{6}$$

The relationship between the vertical movement Δ_{vB} of Point F and Δ_{rB} is

$$\Delta_{vB} = \Delta_{rB} \cos\theta \tag{7}$$

Substituting Eq. (6) into Eq. (7), the relationship between the tensile elongation δ_{tB} of a strip and the vertical movement of the right-hand edge of the shear panel can be derived as

$$\delta_{tB} = \frac{\Delta_{vs} \sin\alpha}{\cos\theta} \tag{8}$$

The internal work done due to the tensile stresses in Region B is

$$W_{Bt} = \Delta_{vs} \int_0^{d\cos(\alpha+\theta)-c\sin\alpha} \sigma_t t \times \frac{\sin\alpha}{\cos\theta} \mathrm{dx} = \Delta_{vs} \sigma_t t [d\cos(\alpha+\theta) - c\sin\alpha] \times \frac{\sin\alpha}{\cos\theta} \tag{9}$$

In Region A in Fig. 8(a), the orientation of the strips in Region A is identical to that of the strips in Region B, and so the relationship between the tensile elongation in Region A and that in Region B is

$$\delta_{tA} = \frac{m}{c} \times \delta_{tB} \tag{10}$$

To obtain the relationship between the tensile elongation δ_{tA} and the vertical edge movement Δ_{vs}, substituting Eq. (10) into Eq. (8), gives

$$\delta_{tA} = \frac{m}{c} \times \frac{\sin\alpha}{\cos\theta} \times \Delta_{vs} \tag{11}$$

The internal work done by the tensile stresses in Region A is given as

$$W_{At} = 2\sigma_t t \int_0^{c\sin\alpha} \frac{m}{c} \times \frac{\sin\alpha}{\cos\theta} \times \Delta_{vs} dx \tag{12}$$

In Region A $m = \dfrac{x}{\sin\alpha}$, and substituting this into Eq. (12) gives

$$W_{At} = \Delta_{vs} \times \frac{2\sigma_t t}{c\cos\theta} \int_0^{c\sin\alpha} x dx = \frac{c\sigma_t t \sin^2\alpha}{\cos\theta} \times \Delta_{vs} \tag{13}$$

The overall internal work done by stretching the entire shear panel is given by summation of W_{At} and W_{Bt}

$$W_T = W_{At} + W_{Bt} = \frac{d\sigma_t t \cos(\alpha+\theta)\sin\alpha}{\cos\theta} \Delta_{vs} \tag{14}$$

3.2.1.2 Case 2

In Case 2, the angle α of the tensile stresses to the upper edge of the panel is equal to γ, as shown in Fig. 7(b).

The internal work done by plastic stretching of the tensile strips can be determined similarly to that of Region A in Case 1. Case 2 has no Region B, and the internal work W_{At} done within Region A is still given by Eq. (13). On the basis of the geometry of this case,

$$c\sin\alpha = d\cos(\alpha+\theta) \tag{15}$$

The overall internal work done by stretching of the shear panel is in this case given as Eq. (14), which turns out to be identical to that of Case 1.

3.2.1.3 Case 3

In Case 3, the angle α is larger than γ, as shown in Fig. 7(c). Again, the panel is divided into two regions A and B, as shown in Fig. 9.

In Region B, for a sample tensile strip EF, the elongation of the strip can be related to the resultant movement of the right-hand edge of the shear panel:

$$\delta_{tB} = \frac{n}{c} \times \sin\alpha \times \Delta_{rs} \tag{16}$$

Based on the relationship, $\Delta_{vs} = \Delta_{rs}\cos\theta$

$$\delta_{tB} = \Delta_{vs} \times \frac{\sin\alpha}{\cos\theta} \times \frac{n}{c} \tag{17}$$

On the basis of geometry, $n = \dfrac{d\cos(\alpha+\theta)}{\sin\alpha}$

The relationship between the tensile elongation of a strip in Region B and the resultant movement of the right-hand edge of the panel Δ_{vs} is

$$\delta_{tB} = \Delta_{vs} \times \frac{\sin\alpha}{\cos\theta} \times \frac{\dfrac{d\cos(\alpha+\theta)}{\sin\alpha}}{c} \tag{18}$$

The internal work done by the tensile stresses in Region B is therefore

$$\begin{aligned} W_{Bt} &= \Delta_{vs}\int_0^{c\sin\alpha - d\cos(\alpha+\theta)} \sigma_t t \times \frac{\sin\alpha}{\cos\theta} \times \frac{\dfrac{d\cos(\alpha+\theta)}{\sin\alpha}}{c} dx \\ &= \Delta_{vs} \times \left[\frac{\sigma_t t d\cos(\alpha+\theta)\sin\alpha}{\cos\theta} - \frac{\sigma_t t d^2\cos^2(\alpha+\theta)}{c\cos\theta}\right] \end{aligned} \tag{19}$$

The internal work of Region A is given as,

$$W_{At} = 2\sigma_t t\int_0^{d\cos(\alpha+\theta)} \frac{m}{c} \times \frac{\sin\alpha}{\cos\theta} \times \Delta_{vs} dx \tag{20}$$

In Region A, $m = \dfrac{x}{\sin\alpha}$, and substituting this into Eq. (20) gives

$$W_{At} = \Delta_{vs} \times \frac{2\sigma_t t}{c\cos\theta}\int_0^{d\cos(\alpha+\theta)} x dx = \frac{\sigma_t t d^2\cos^2(\alpha+\theta)}{c\cos\theta} \times \Delta_{vs} \tag{21}$$

Then adding W_{At} and W_{Bt} gives the total internal work done by plastic stretching of the shear panel in this case.

$$W_T = \frac{d\sigma_t t \cos(\alpha+\theta)\sin\alpha}{\cos\theta}\Delta_{vs} \tag{22}$$

It can be seen that the formulation of the internal work done by tension turns out to be the same for all the three cases. This shows that the tensile resistance of a shear panel is not sensitive to the locations of plastic hinges.

For compressive strips, there are also three cases depending on the locations of plastic hinges. Similarly to the tensile resistance, it can also be proved that the compressive capacity of a shear panel is not sensitive to the locations of the plastic hinges. For all three cases, the formulation of the internal work of the compressive strips is identical, and is given as

$$W_C = \frac{d\sigma_c t \sin(\alpha+\theta)\cos\alpha}{\cos\theta}\Delta_{vs} \tag{23}$$

Therefore, the internal work of the web in the post-buckling stage is

$$W_W = W_T + W_C = \frac{d\sigma_t t \cos(\alpha+\theta)\sin\alpha}{\cos\theta}\Delta_{vs} + \frac{d\sigma_c t \sin(\alpha+\theta)\cos\alpha}{\cos\theta}\Delta_{vs} \tag{24}$$

3.2.2 Internal work of the top and bottom flanges

The internal work of the flanges is the work done in deforming the four plastic hinges on the top and bottom flanges of the beam. The plastic moment resistance of each of the four hinges is

$$M_0 = \frac{1}{4} f_{y,\theta} b_f t_f^2 \tag{25}$$

In this equation M_0 does not account for the effect of the axial stresses in the flanges caused by bending of the overall beam cross-section, which reduces the flange moment capacity. The reduced moment capacity due to overall bending is given as

$$M_1 = M_0[1-(\frac{\sigma_{t(c)}}{f_{y,\theta}})^2] = \frac{1}{4} f_{y,\theta} b_f t_f^2 [1-(\frac{M_r \times \frac{1}{2}(d+\frac{1}{2}t_f)}{If_{y,\theta}})^2] \quad (M_1 \geq 0)$$

$$M_1 = 0 \qquad (M_1 < 0) \tag{26}$$

The internal work done by the plastic hinges in the flanges is therefore

$$W_f = 4M_1\theta = f_{y,\theta} b_f t_f^2 [1-(\frac{\frac{1}{2}M_r(d+\frac{1}{2}t_f)}{If_{y,\theta}})^2]\theta \tag{27}$$

3.2.3 Total internal work of the beam

The analytical model can calculate the distance between the plastic hinges on the flanges. The calculated value indicates whether plastic hinges have been formed; positive values indicate the occurrence of plastic hinges, whereas negative or imaginary values mean the opposite. If plastic hinges have been formed, the internal work done by the beam is given by summation of the work done in the beam web and flanges. Otherwise, the internal work is solely that of the beam web.

As discussed is Section 3, there are three key points to decide the theoretical force-deflection relationship. Point 1 is the end of elastic range, Point 2 refers to the initiation of buckling, and Point 3 represents failure. It is assumed that, at the initial buckling point (Point 2), the compressive stresses in the beam web have not been decreased due to the effect of buckling. Therefore, the tensile and compressive stresses are equal:

$$\sigma_t = \sigma_c \tag{28}$$

Using the Huber-von Mises plasticity criterion [26], the relationship between the tensile and compressive stresses for a two-dimensional panel is

$$\sigma_c^2 + \sigma_t^2 + (\sigma_t - \sigma_c)^2 = 2f_{y,\theta}^2 \tag{29}$$

Substituting Equations (28) and (29) into Eq. (24), the internal work of the web panel is

$$W_W = \frac{f_{y,\theta} dt \sin(2\alpha + \theta)}{\sqrt{3}\cos\theta} \Delta_{vs} \tag{30}$$

If plastic hinges occur, the internal work of the flanges can be calculated according to Eq. (27).

Beyond the buckling point, the shear panel enters the post-buckling stage. For Point 3 in Fig. 4, the post-buckling strength reduction is accounted for by reduction of the compressive stresses in the compressive strips. In the post-buckling stage, the compressive strips are considered as struts with three plastic hinges, as shown in Fig. 10.

It has been assumed that the central plastic hinge always forms at the mid-length of each strut, although this assumption may lead to an out-of-plane deflection shape, which is slightly different from reality. For each strut shown in Fig. 10, the rectangular cross section can be divided into two parts, as shown in Fig. 11. The axial compressive strength of the strut is resisted by Region A and its bending moment resistance is provided by Region B. Therefore,

$$P_c = \sigma_c h_c f \tag{31}$$

$$M_p = \frac{1}{4} f (t^2 - h_c^2) \sigma_c \tag{32}$$

Based on force equilibrium, the relationship between the compression force P_c of the strut and the plastic moment M_p at the plastic hinge is

$$P_c \Delta = 2M_p \tag{33}$$

Substituting Equations (31) and (32) into Eq. (33), the height h_c of the compression zone can be calculated. The reduced compressive stress σ_c is proportional to h_c, which gives

$$\sigma_c = \frac{h_c}{t} f_{y,\theta} \tag{34}$$

Following Eq. (29), for any reduced σ_c, the tensile stress σ_t can be calculated. Both σ_c and σ_t are proportional to the yield strength. A and B in Eq. (35) are the ratios of σ_c and σ_t to $f_{y,\theta}$, respectively. A and B have already been achieved from Eq. (29) and Eqs. (32)-(34). Therefore, the high-temperature yield strengths can be defined as

$$\sigma_c = Af_{y,\theta} \text{ and } \sigma_t = Bf_{y,\theta} \tag{35}$$

Substituting Eq. (35) into Eq. (24) gives

$$\begin{aligned} W_W &= W_T + W_C = \frac{\sigma_t td \sin\alpha\cos(\alpha+\theta) + \sigma_c td \sin(\alpha+\theta)\cos\alpha}{\cos\theta}\Delta_{vs} \\ &= \frac{Af_{y,\theta}td \sin\alpha\cos(\alpha+\theta) + Bf_{y,\theta}td \sin(\alpha+\theta)\cos\alpha}{\cos\theta}\Delta_{vs} \\ &= \frac{f_{y,\theta}td}{\cos\theta}[\frac{1}{2}(A+B)\sin(2\alpha+\theta) + \frac{1}{2}(B-A)\sin\theta]\Delta_{vs} \end{aligned} \tag{36}$$

As has been presented in 3.1, for each c the transverse drift Δ_{vs} of the shear panel can be calculated. This can influence the reduction of compressive stress, which in return changes the calculated value of the distance between the plastic hinges. Therefore, an iterative process is used here to balance the value of c.

3.3 External work

If a beam is subjected to uniformly distributed load, the external work is given as

$$W_e = \frac{1}{2}cq\Delta_{vs} + q(l-c)\Delta_{vs} = q(l-\frac{1}{2}c)\Delta_{vs} \tag{37}$$

It has been explained above that internal work is only related to the distance c between plastic hinges, rather than the length of the shear buckling wave. This is also the case for the external work, as indicated by Eq. (37).

4. Validation against finite element modelling

In this study, the S4R element of ABAQUS [27] was adopted. This is a four-noded shell element which is capable of simulating buckling behaviour with reasonable accuracy. A mesh sensitivity analysis was carried out, and a 20mm x 20mm element size was selected to achieve optimum accuracy and efficiency. Riks analysis was used to track the descending load path of the shear panel in the post-buckling stage. An initial imperfection of amplitude $d/200$ (complying with Eurocode 3 Part 1-5 [28]) was adopted. The shape of the initial imperfection was based on a first-buckling-mode analysis. Fig. 12(a) shows the finite element model of an isolated Class 1 beam. Six cases were analysed using different beam lengths with identical cross sections, at temperatures of 20^{o}C, 500^{o}C, 600^{o}C and 700^{o}C. The dimensions of the cross section are shown in Fig. 12(c). The same material properties used for the analytical model (illustrated in Fig. 5) were applied. The detailed material properties used in both the FE and analytical models are shown in Table 1. To save computing time, only half of a beam was modelled. The beam is fixed at one end. The other end of the FE model, which is the mid span of the beam, is allowed to move vertically without any rotation due to symmetry. As the effects of axial force caused by thermal expansion has not been considered in the analytical model, the mid span is allowed to move horizontally in the FE model. Boundary conditions are shown in Fig. 12(b).

The force-displacement relationships given by the analytical model and the ABAQUS analysis are compared in Fig. 13, at temperatures varying from 20^{o}C to 700^{o}C. The solid lines represent ABAQUS results, whereas the three round markers in each part of this figure show Points 1 to 3 given by the analytical model. As can be seen from Fig. 13, the beam-end reaction forces given by the analytical model generally compare well with those from the

ABAQUS model at all three stages. The theoretical results are always on the safe side for the cases analysed.

The distances c between plastic hinges for different beam lengths, given by the analytical model, are shown in Fig. 14. The distance c does not change with temperature. Therefore, for a particular beam length only one distance between plastic hinges has been derived for any temperature. The solid line represents the variation of c with beam length at Point 2, and the dashed line is that for Point 3. The values of c for both Points 2 and 3 are positive definite for beams shorter than 5m. This means that the plastic hinges have been formed before beam web buckling occurs. For beams of lengths between 5-6m, the value of c at Point 2 doesn't exist, whereas that for Point 3 remains positive. This means that plastic hinges are formed on the flanges after the beam web buckles. These results can not be validated by FE modelling; even if plastic hinges occur on the flanges, the rotations across the hinges will be too small to be observed. For all beams shorter than 6m, failure is controlled by the shear buckling of the beam web. As the beam length increases, the distances between plastic hinges for both Points 2 and 3 are imaginary. This means that plastic hinges do not form and shear buckling does not occur. This shift of failure mode is also observed from the ABAQUS model, as shown in Fig. 15 and 16. Fig. 15 is a contour plot of the out-of-plane deflection of a representative 3m beam. The formation of plastic hinges and beam-web shear buckling are obvious from this figure. The same phenomenon occurs to beams of lengths between 3.5m and 5.5m. Fig. 16 is a contour plot of out-of-plane deflection for a 6m beam, which fails by bottom-flange buckling rather than by shear buckling of the beam web. This may be caused by an increasing level of compressive stress, due to bending, in the bottom flanges as the beam length increases, which causes the bottom-flange buckling to occur prior to beam-web shear buckling. The bottom-flange

buckling causes rotation of the beam about its ends, which can lead to large mid-span vertical deflection for a long beam. Although the tendency for bottom-flange buckling to occur increases as beam length increases, it has not been included in the current analytical model. This explains the reason for the relatively larger discrepancies in vertical deflection of the longer beams between the theoretical and ABAQUS models, as shown in Fig. 13.

5. Conclusions

A brief review of tension field theory [9-11, 14-16] in terms of web shear buckling in plate girders has been presented. The primary goal has been to create a simplified analytical model for shear buckling behaviour of Class 1 beams based on tension field theory.

An analytical model has been created to predict the shear capacity and vertical deflection of shear panels at both ambient and elevated temperatures. The analytical model is capable of predicting the formation of plastic hinges on flanges, the initiation of beam-web shear buckling and the failure point for Class 1 beams. A tri-linear curve can be created by linking these three points, in order to track the load-deflection route of the shear panel. A new component-based shear panel element, which considers the shear panel as a separate component, will be created based on the analytical model.

The theoretical results have been validated against finite element modelling using ABAQUS over a range of geometries. For beams for which beam-web shear bucking is the main 'failure' mode, the comparisons between the theoretical and FE models have shown that the proposed method provides satisfactory accuracy in terms of both shear capacity and mid-span vertical deflection. However, as beam length increases, the 'failure' mode switches to bottom-flange buckling. This phenomenon can be observed from the ABAQUS

models. As bottom-flange buckling has not been involved in the analytical model so far, the discrepancies between the two models tend to become larger as beam length increases.

In future work, axial forces caused by restraint to thermal expansion of the beam will be added to the component-based analytical model of the shear panel. An analytical model of bottom-flange buckling at high temperatures will then be created. Together with the beam-web shear buckling model, the analytical models will at that stage work well over a large range of beam lengths. The analytical models will be implemented in the software *Vulcan*, and in due course will be used in global modelling of composite structures in fire.

References

[1] Gann RG. Final Report on the Collapse of World Trade Center Building 7,Federal Building and Fire Safety Investigation of the World Trade Center Disaster. Gaithersburg, US: The National Institute of Standards and Technology (NIST); 2008.
[2] Da Silva LS, Real AS, Vila P, Moore D. Behaviour of steel joints under fire loading. Steel & Composite Structures. 2005;5:485-513.
[3] Al-Jabri KS, Davison JB, Burgess IW. Performance of beam-to-column joints in fire—a review. Fire Safety Journal. 2008;43:50-62.
[4] Burgess I, Davison JB, Dong G, Huang S-S. The role of connections in the response of steel frames to fire. Structural Engineering International. 2012;22:449-61.
[5] Newman G, Robinson JT, Bailey CG. Fire safe design: A new approach to multi-storey steel-framed buildings. SCI publication. 2001;288.
[6] CEN. BS EN 1993-1-1. Design of steel structures. Part 1.1: General structural rules. UK: British Standards Institution; 2005.
[7] Wilson JM. On specifications for strength of iron bridges. Transactions of the American Society of Civil Engineers. 1886;15:389-414.
[8] Wagner H. Flat sheet metal girder with very thin metal web: National Advisory Committee for Aeronautics; 1931.
[9] Basler K, Yen B, Mueller J, Thurlimann B. Web buckling tests on welded plate girders: Fritz Engineering Laboratory, Lehigh University; 1960.
[10] Basler K. Strength of plate girder in shear. Journal of the Structural Division ASCE. 1961;87(ST7):151-80.
[11] Basler K. Strength of plate girder under conbined bending and shear. Journal of the Structural Division ASCE. 1961;87(ST7):181-97.
[12] ASIC. Specification for the design, fabrication and erection of structural steel for building: American Institute of Steel Construction; 1963.
[13] Fujii T. On an improved theory for Dr. Basler's theory. Proceeding of 8th Congress, IABSE, New York1968. p. 477-87.
[14] Rockey K, Skaloud M. Influence of flange stiffness upon the load carrying capacity of webs in shear. 8th Congress of IABSE, Final Report, New York1968.

[15] Rockey K, Skaloud M. The ultimate load behaviour of plate girders loaded in shear. Struct Eng. 1972;50:29-47.
[16] Rockey K, Evans H, Porter D. A design method for predicting the collapse behaviour of plate girders. ICE proceedings: Ice Virtual Library; 1978. p. 85-112.
[17] Porter D, Rockey K, Evans H. The collapse behaviour of plate girders loaded in shear: University College Department of Civil and Structural Engineering; 1987.
[18] Galambos TV. Guide to stability design criteria for metal structures: Structure Stability Research Council; 1998.
[19] Lee SC, Lee DS, Yoo CH. Ultimate shear strength of long web panels. Journal of Constructional Steel Research. 2008;64:1357-65.
[20] Lee SC, Yoo CH. Strength of plate girder web panels under pure shear. Journal of Structural Engineering. 1998;124:184-94.
[21] Yoo CH, Lee SC. Mechanics of web panel postbuckling behavior in shear. Journal of Structural Engineering. 2006;132:1580-9.
[22] Vimonsatit V, Tan K, Qian Z. Testing of plate girder web panel loaded in shear at elevated temperature. Journal of Structural Engineering. 2007;133:815-24.
[23] Vimonsatit V, Tan K-H, Ting S-K. Shear strength of plate girder web panel at elevated temperature. Journal of Constructional Steel Research. 2007;63:1442-51.
[24] Timoshenko SP, Gere JM. Theory of elastic stability. 1961. McGraw-Hill, New York; 1961.
[25] CEN. BS EN 1993-1-2. Design of steel structures. Part 1.2: General rules — Structural Fire Design. UK: British Standards Institution; 2005.
[26] Hencky H. Zur Theorie plastischer Deformationen und der hierdurch im Material hervorgerufenen Nachspannungen. ZAMM ‐ Journal of Applied Mathematics and Mechanics/Zeitschrift für Angewandte Mathematik und Mechanik. 1924;4:323-34.
[27] Hibbit D, Karlsson B, Sorenson P. ABAQUS reference manual 6.7. Pawtucket: ABAQUS Inc; 2005.
[28] CEN. Eurocode 3: Design of steel structures. Part 1.5: Plated structural elements. 2006.

List of Tables

Table1. Material Properties

List of Figure Captions

Fig. 1. Shear buckling phenomenon in Cardington Fire Test [5]

Fig. 2. Component-based model with the new Shear-panel Component

Fig. 3. Comparisons of web panel behaviour for plate girders and Class 1 beams under shear and bending

Fig. 4. Schematic tri-linear force-deflection curve of a shear panel

Fig. 5. Stress-strain relationship of structural steel [25]; (a) at ambient temperature; (b) at elevated temperatures

Fig. 6. Representative strip and arbitrary point

Fig. 7. Possibilities for the position of plastic hinges; (a) Case 1; (b) Case 2; (c) Case 3

Fig. 8. Case 1: (a) Geometric relationship; (b) Movement relationship in Region B

Fig. 9. Case 3: (a) Geometric relationship; (b) Movement relationship in Region B

Fig. 10. Struts representing compressive strips

Fig. 11. Cross section of one strut

Fig. 12. Finite element model; (a) Image of finite element model; (b) Boundary conditions; (c) Cross section dimensions (in mm)

Fig. 13. Comparison of force-displacement curves between ABAQUS and theoretical analysis

Fig. 14. Distance between plastic hinges calculated from the analytical model

Fig. 15. Shear buckling of 3m beam

Fig. 16. Bottom flange buckling of 6m beam

Table 1

Click here to download Table: Table 1.docx

σ_y (N/mm^2)	$\varepsilon_{y,\theta}$ (%)	$\varepsilon_{t,\theta}$ (%)	$\varepsilon_{u,\theta}$ (%)	E (N/mm^2)
275	2	15	20	2.10×e^5

Figure 1

Click here to download Figure: Fig. 1.docx

Figure 2

Click here to download Figure: Fig. 2.docx

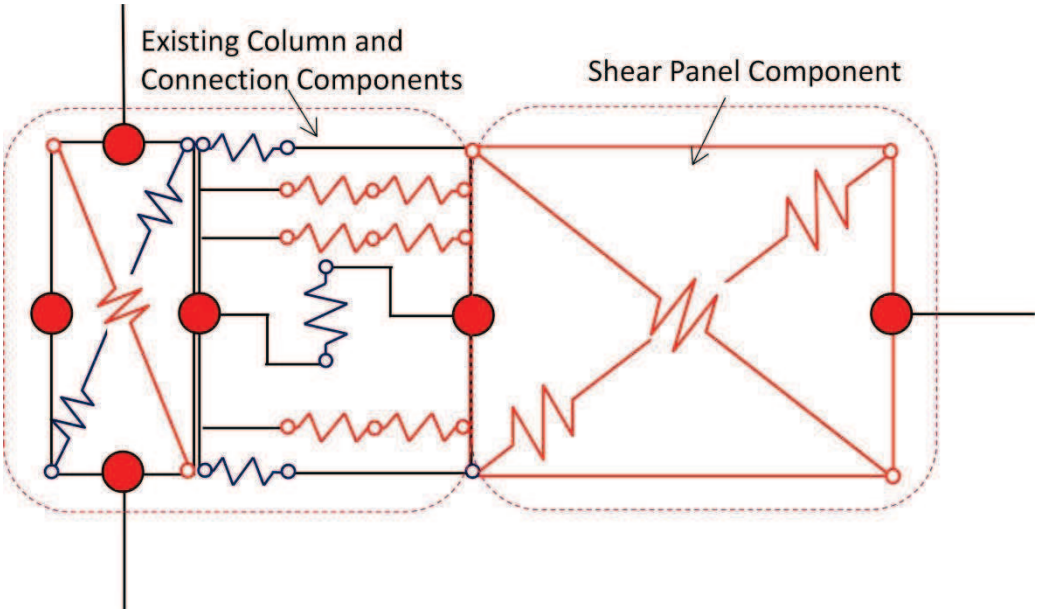

Figure 3
Click here to download Figure: Fig. 3.docx

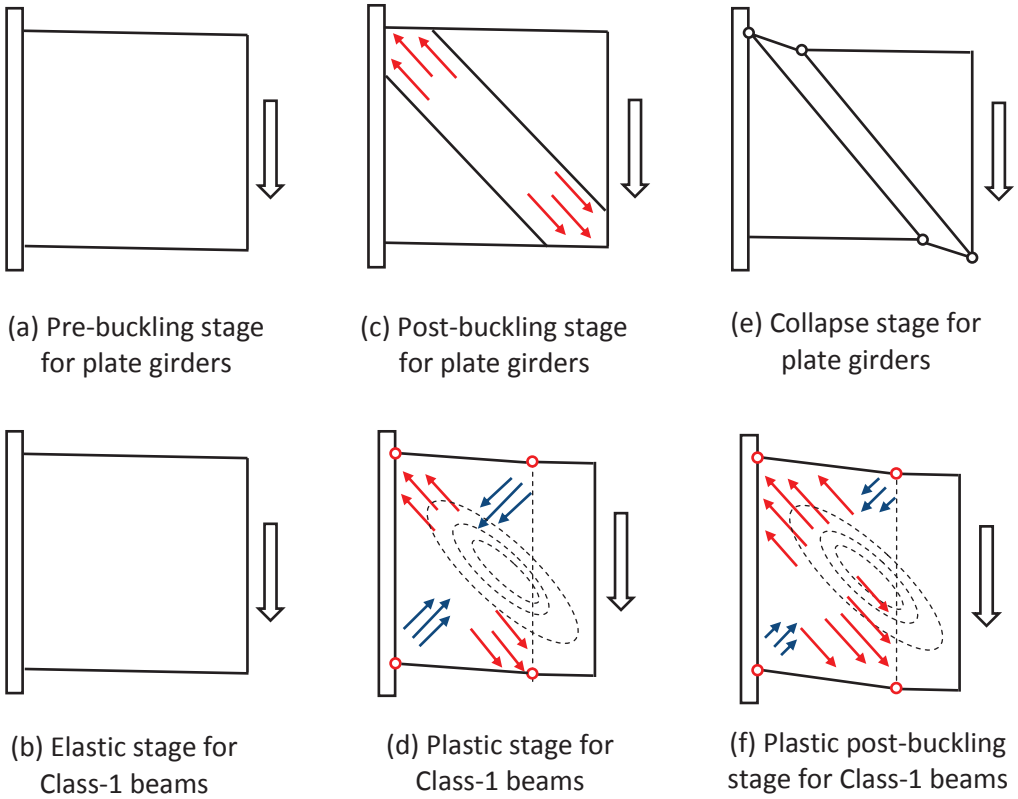

Figure 4

Click here to download Figure: Fig. 4.docx

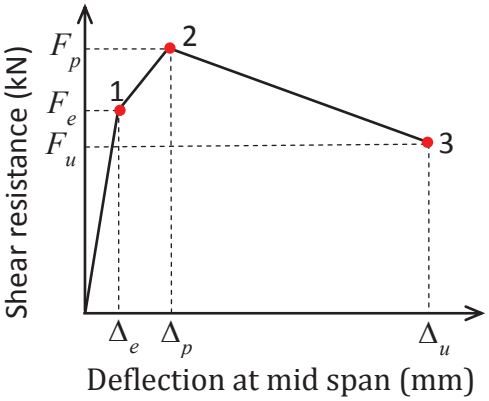

Figure 5

Click here to download Figure: Fig. 5.docx

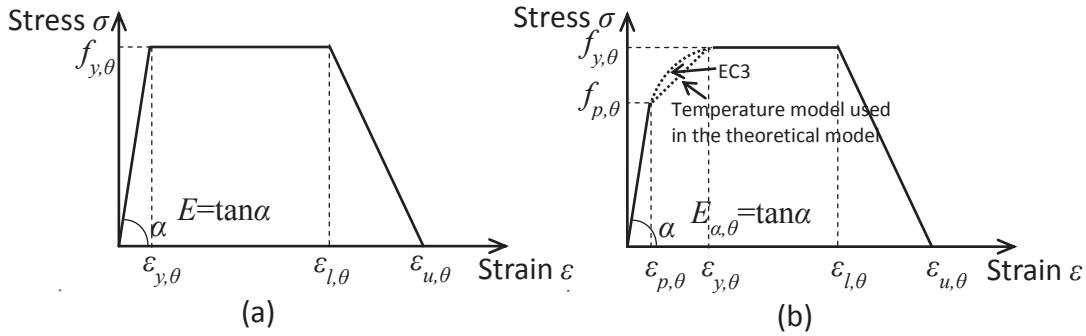

Figure 6

Click here to download Figure: Fig. 6.docx

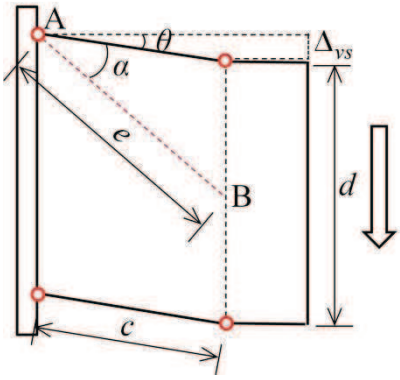

Figure 7

Click here to download Figure: Fig. 7.docx

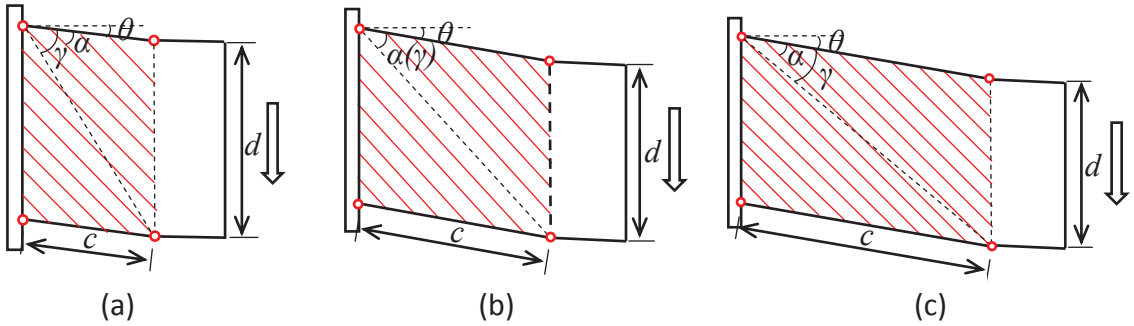

Figure 8
Click here to download Figure: Fig. 8.docx

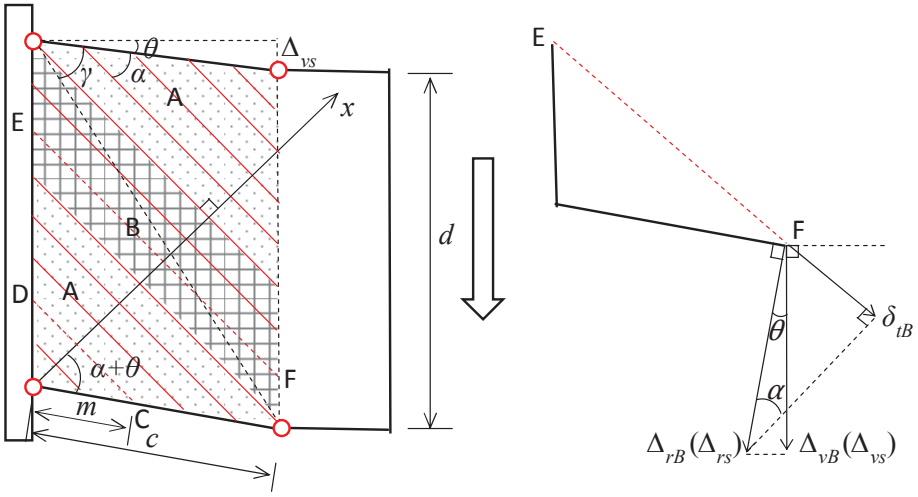

(a) (b)

Figure 9

Click here to download Figure: Fig. 9.docx

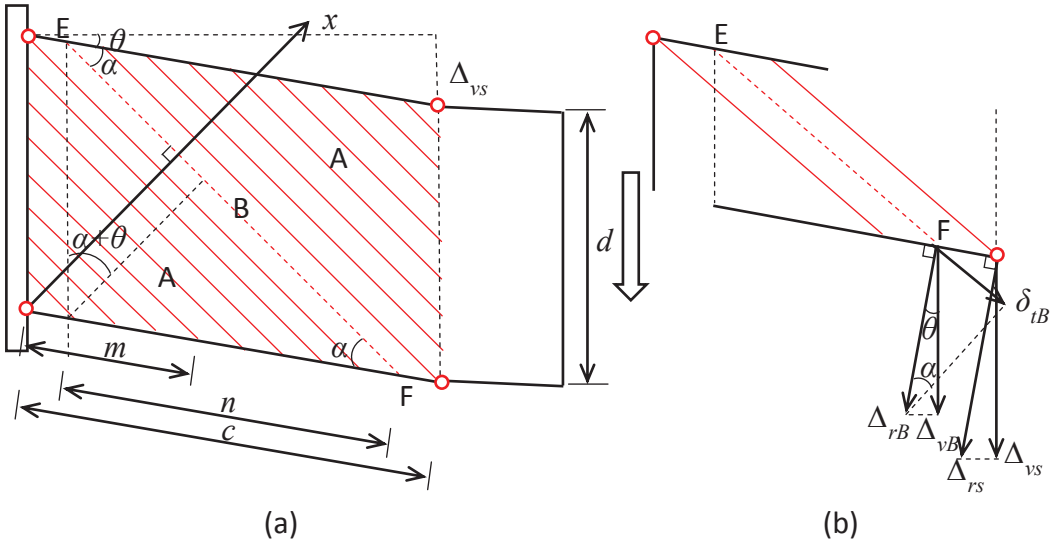

(a) (b)

Figure 10

Click here to download Figure: Fig. 10.docx

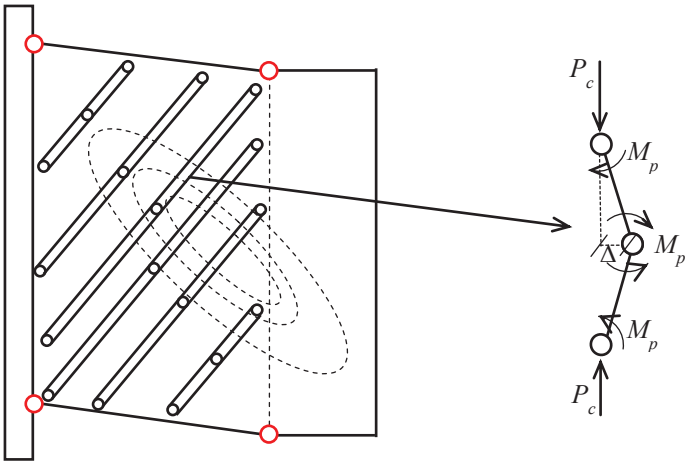

Figure 11
Click here to download Figure: Fig. 11.docx

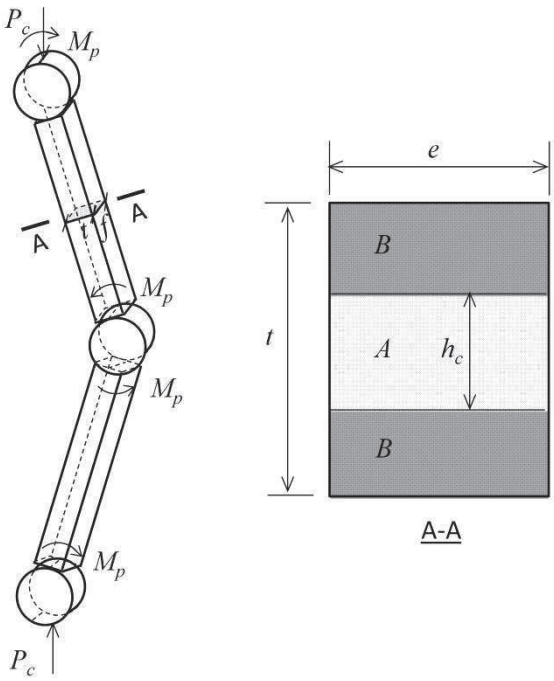

Figure 12
Click here to download Figure: Fig. 12.docx

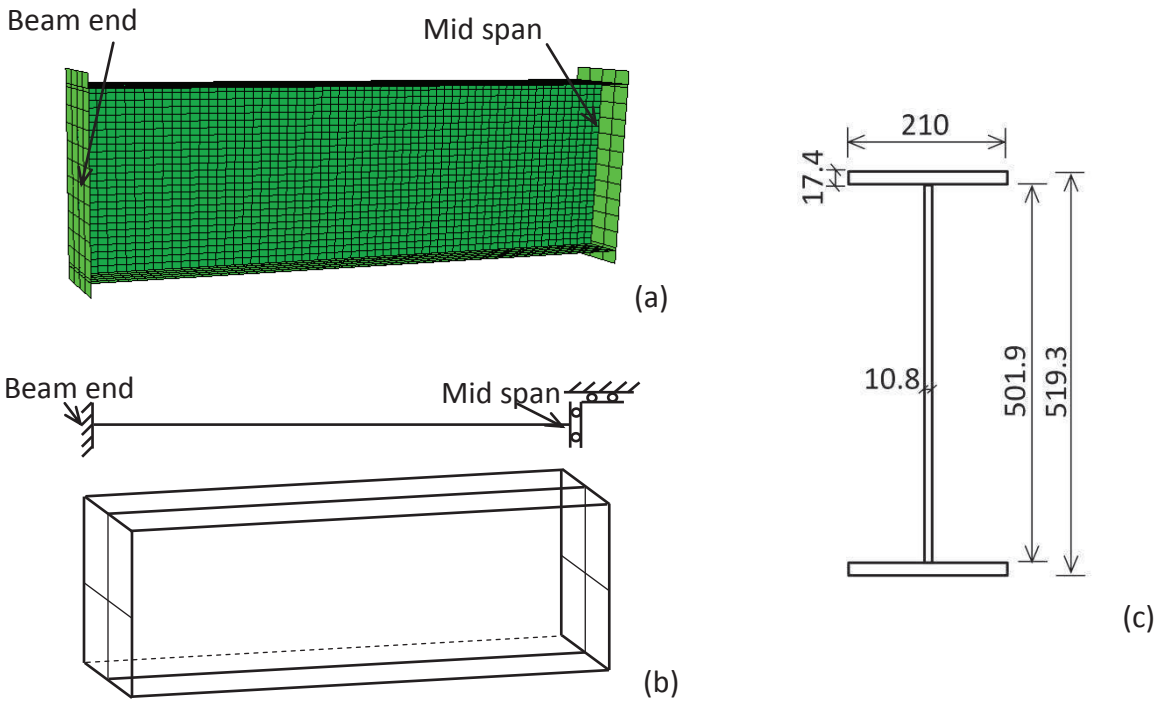

Figure 13

Click here to download Figure: Fig. 13.docx

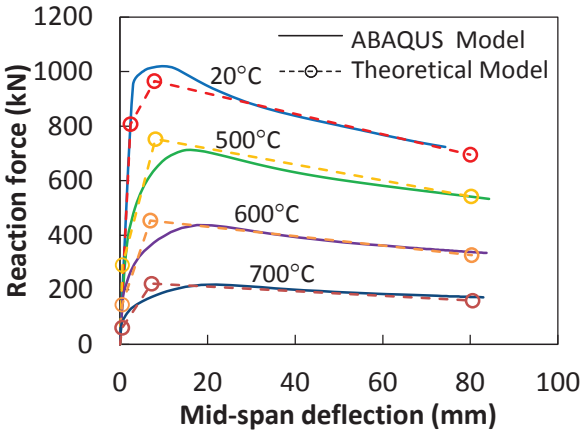

Beam length=3000mm

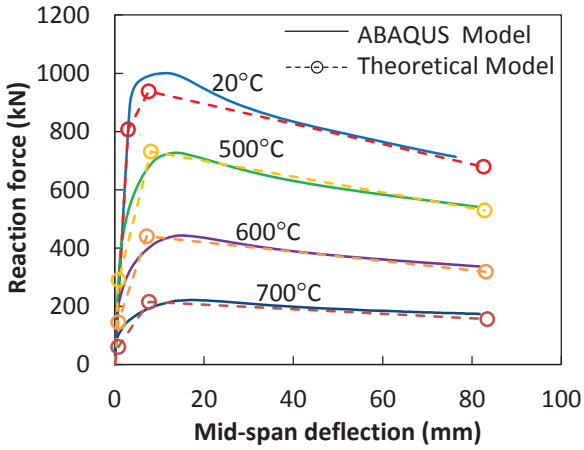

Beam length=3500mm

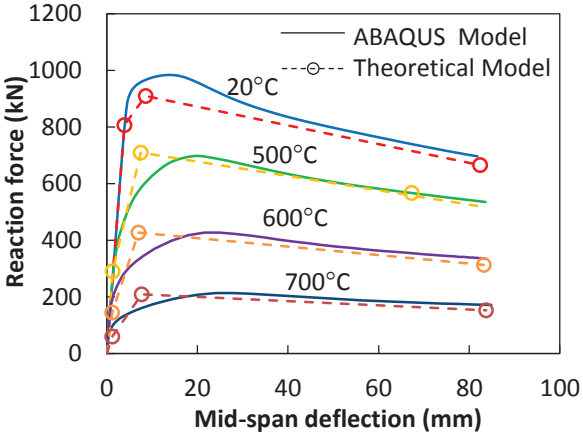

Beam length=4000mm

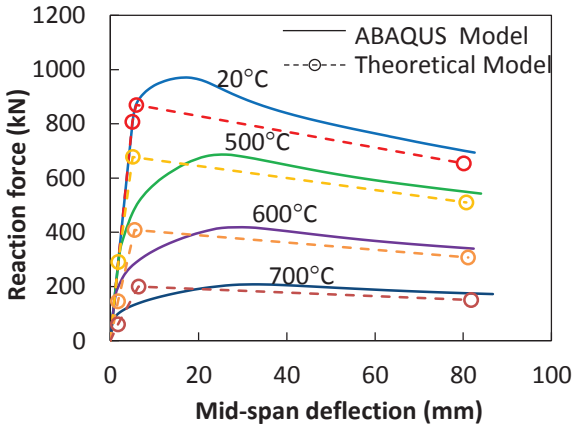

Beam length=4500mm

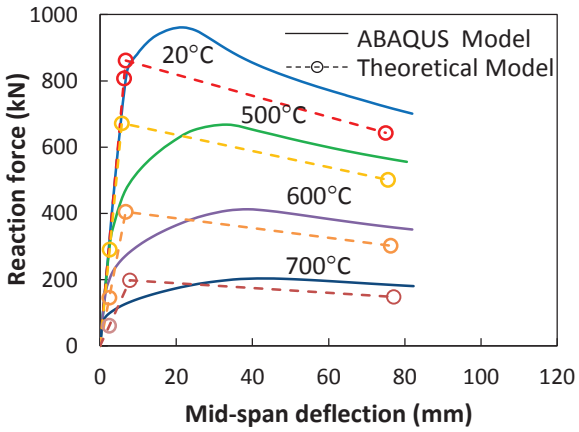

Beam length=5000mm

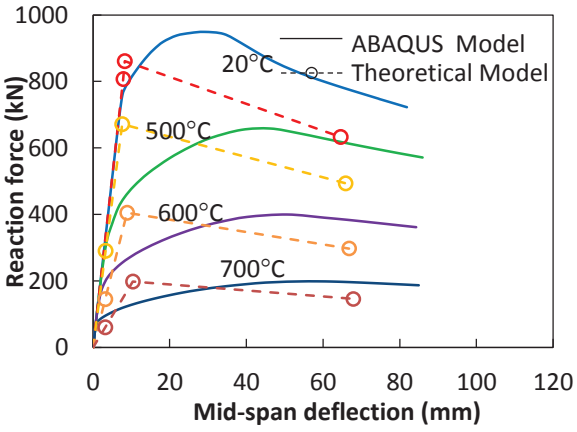

Beam length=5500mm

Figure 14

Click here to download Figure: Fig. 14.docx

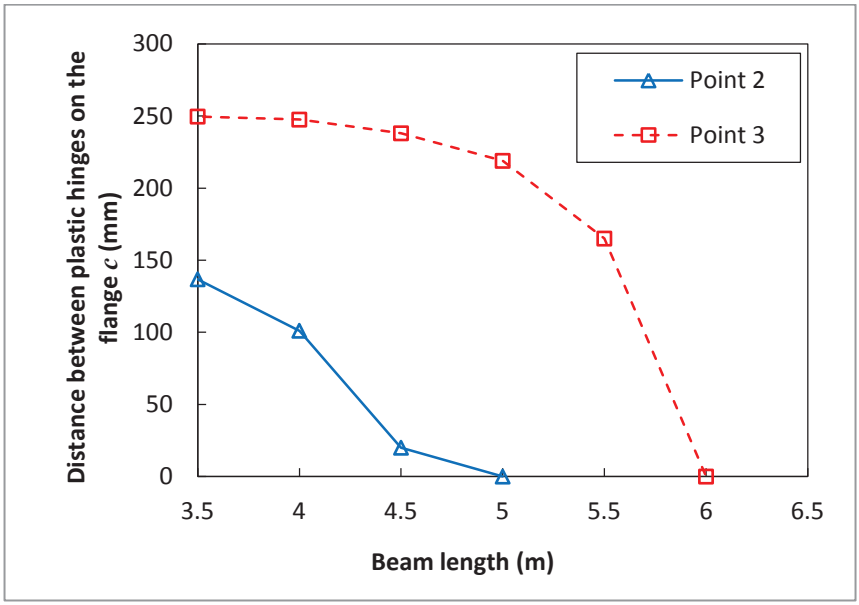

Figure 15
Click here to download Figure: Fig. 15.docx

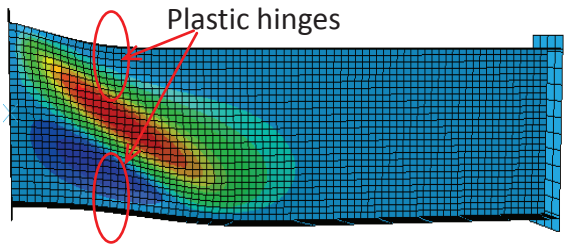

Figure 16

Click here to download Figure: Fig. 16.docx